JOURNAL OF COMPUTATIONAL PHYSICS 40, 91–103 (1981)

Numerical Radiation Boundary Conditions for Unsteady Transonic Flow

BJORN ENGQUIST*

Department of Mathematics, University of California, Los Angeles, California 90024

AND

ANDREW MAJDA†

Department of Mathematics, University of California, Berkeley, California 94720

Received March 23, 1979; revised July 8, 1980

A family of numerical boundary conditions for far-field computational boundaries in calculations involving unsteady transonic flow is devised. These boundary conditions are developed in a systematic fashion from general principles. Both numerical and analytic comparisons with other currently used methods are given.

INTRODUCTION

Unsteady transonic flow occurs and its effects are important in many applications such as fluttering airfoils, helicopter blades, turbines, and maneuvering flight (see [1, 2, 5]). The basic small disturbance equation governing unsteady transonic flow (see [5]) is given by

$$2\varphi_{xt} = (K - (\gamma + 1)\varphi_x)\varphi_{xx} + \varphi_{yy}. \tag{0.1}$$

In numerical calculations involving transonic phenomena, typically the computational region is as depicted in Fig. 1. The slit along the x-axis determines the airfoil location where physical boundary conditions are imposed and the walls, $y = \pm b$, $x = 0, a$, are computational boundaries with location determined by computer storage and accuracy requirements, etc. For the computational walls, easily implemented artificial boundary conditions are needed so that the (unphysical) effect of these walls on the computed solution is minimized.

For essentially steady state calculations in transonic flow (when the time dependent term in (0.1) is small), coordinate mapping techniques are a traditional and effective way of handling these computational boundaries. The theoretical reason

* Partially supported by the Swedish Natural Science Research Council (NFR 2711–018).
† Partially supported by a Sloan Foundation Fellowship and NSF Grant MCS 76-10227.

0021-9991/81/030091-13$02.00/0

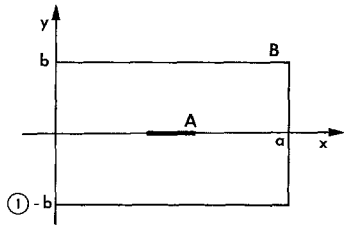

FIG. 1. Computational region for transonic flow. A. Physical boundary. B. Computational boundary ($x = 0, a$; $y = \pm b$).

for the success of coordinate mapping techniques under these circuymstances lies in the fact that the steady state far-field asymptotic behavior is given by a regular algebraic singularity without oscillations (see [3, p. 774]). On the other hand, when one is interested in genuinely unsteady transonic phenomena, solutions of (0.1) possess a strong oscillatory transient behavior and the far-field asymptotic behavior is oscillatory with essential singularities (see [5]). Under such conditions, coordinate mapping techniques are ineffective (see [4]) and one needs an alternative procedure for treating the computational boundaries. Similar remarks apply (see pp. 288–289 of [4]) when coordinate stretching techniques near infinity are applied to problems with oscillatory behavior.

In [6, 7], the authors introduced and developed a systematic technique for designing radiating boundary conditions at computational boundaries to be used when highly oscillatory transient phenomena are computed. Here we apply these techniques to the computational boundaries of unsteady small disturbance, transonic flow (depicted as $y = \pm b$, $x = 0, a$ in Fig. 1). The application involves the assessment of two new difficulties not treated in [6, 7],

(0.2)
(1) Waves propagate with essentially infinite speed when striking the $y = \pm b$ boundaries so that a proper assessment of "glancing effects" is crucial.
(2) The equation in (0.1) is nonlinear.

The effects in (1) are more significant than those in (2) for the farfield boundaries, especially, when the flow is subsonic in the farfield. First, as background, we discuss well-posed far-field boundary conditions for (0.1) and describe the far-field boundary procedures used by Krupp and Cole (see [5]) and Ballhaus and Goorjian (see [1]). Then, we design practical radiation boundary conditions for (0.1) and present several strategies for treating the new difficulties in (0.2) above—the "best" strategy, of course, is problem dependent. We also provide analytic comparisons between the boundary conditions used in [1, 5], and the ones developed here. Finally, we discretize the boundary conditions and present numerical comparisons of these methods and those used in [1, 5]. We concentrate only on the errors introduced by the computational boundaries, B, in Fig. 1.

In view of applications, we emphasize the far-field subsonic case below but also include a discussion of the supersonic case. The radiating boundary conditions for (0.1) which we construct here have obvious generalizations for the equations of three-dimensional unsteady small disturbance transonic flow.

1. Well-Posed Far-Field Boundary Conditions

We define K^* by $K^* \equiv K - (\gamma + 1)\varphi_x$; the flow is locally *subsonic* (supersonic) when $K^* > 0$ ($K^* < 0$). The equation in (0.1) becomes

$$2\varphi_{xt} = K^*\varphi_{xx} + \varphi_{yy}. \tag{1.1}$$

We assume that K^* is (locally) a fixed constant in the (local) stability analysis presented below. We use the energy method for boundary conditions of the form,

$$\varphi_y - a\varphi_x|_B = 0 \qquad \text{or} \qquad \varphi|_B = 0 \qquad \text{or} \qquad \varphi_x|_B = 0 \tag{1.2}$$

and ignored the physical boundary, A, since correct boundation conditions are well known. Stability for the higher order radiating boundary conditions developed in Section 2 can only be determined by more sophisticated normal mode analysis (see [6, 7]), or numerical experiments. We use the x-component of kinetic energy as a natural measure of stability and determine the boundary conditions satisfying,

$$\frac{\partial}{\partial t}\int_{-b}^{b}\int_{0}^{a}(\varphi_x)^2\,dx\,dy \leqslant 0. \tag{1.3}$$

We compute by integration by parts and (1.1) that

$$\frac{\partial}{\partial t}\int_{-b}^{b}\int_{0}^{a}(\varphi_x)^2\,dx\,dy = \tfrac{1}{2}\int_{x=a}(K^*\varphi_x^2 - \varphi_y^2)\,dy$$
$$-\tfrac{1}{2}\int_{x=0}(K^*\varphi_x^2 - \varphi_y^2)\,dy + \int_{y=b}\varphi_x\varphi_y\,dx - \int_{y=-b}\varphi_x\varphi_y\,dx. \tag{1.4}$$

By substituting boundary conditions of the form in (1.2) into (1.4) and verifying the stability criteria of (1.3), we obtain the following list of simple well-posed boundary conditions (others exist via normal mode analysis):

Downstream: $(x = a)$

$$\varphi_y - c\varphi_x|_{x=a} = 0, \qquad \text{where } c^2 \geqslant K^*.$$
$$\varphi_x|_{x=a} = 0.$$

Upstream: $(x = 0)$ (1.5)

$$(\varphi_y - c\varphi_x)|_{x=0} = 0, \quad \text{where } c^2 \leqslant K^*,$$
$$\varphi|_{x=0} \equiv 0.$$

Sidewalls: $(y = \pm b)$

$$\varphi_x - c_1\varphi_y|_{y=b} = 0, \quad c_1 \leqslant 0, \qquad \varphi_x - c_2\varphi_y|_{y=-b} = 0, \quad c_2 \geqslant 0,$$
$$\varphi|_{y=b} = 0, \qquad \varphi|_{y=-b} \equiv 0,$$
$$\varphi_x|_{y=b} = 0, \qquad \varphi_x|_{y=-b} = 0.$$

The far-field boundary conditions used by Ballhaus and Goorjian in [1] are (only for the *subsonic* case)

$$\begin{aligned} \varphi &= 0, \quad \text{on upstream and side walls,} \\ \varphi_x &= 0, \quad \text{downstream.} \end{aligned} \tag{1.6}$$

The far-field boundary conditions used by Krupp and Cole in [5] are the same as those in (1.6) except they also implemented (a discrete version of) the boundary condition

$$\varphi_{xx}|_{x=a} = 0, \quad \text{downstream.} \tag{1.7}$$

Krupp and Cole mention the possibility of using a far-field fundamental-solution for the periodic motions studied in [5] but did not implement such an approach in their computational algorithms.

While the boundary condition, $\varphi = 0$ on upstream and side walls, is well posed, the analysis and numerical experiments in the next sections indicate that these conditions are "perfectly reflecting" rather than "radiating," they are a poor choice for the far-field boundaries.

2. Design of Radiating Boundary Conditions

The design of effective far-field radiation boundary conditions depends on the wave propagation properties of the equation

$$2\varphi_{xt} = K^*\varphi_{xx} + \varphi_{yy}, \tag{2.1}$$

where K^* is a fixed constant. Given a unit vector, $\boldsymbol{\omega} = (\omega_1, \omega_2)$, the equation in (2.1) has plane wave solutions, $f(ct - x\omega_1 - y\omega_2)$, with local wave speed given by

$$c = -\frac{K^*\omega_1^2 + \omega_2^2}{2\omega_1}. \tag{2.2}$$

From (2.2) it follows that the speed of propagation is arbitrarily large in the unit directions, $\boldsymbol{\omega} = (\omega_1, \omega_2)$ as $\omega_1 \to 0$. As remarked in [1, 5], a point source, in the subsonic case, $K^* > 0$, generates a parabolic wave front as described in Fig. 2. The design considerations for radiation boundary conditions vary for the side walls,

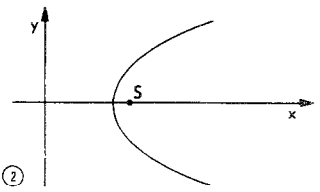

FIG. 2. Wave front generated by a point source S ($K^* > 0$).

upstream, and downstream boundaries, respectively. Because signals generated in the interior and their reflections from the boundaries spread more quickly in the y-direction than in the negative x-direction, the design of effective boundary conditions for the side wall is most important.

Radiation Boundary Conditions for the Side Walls, $y = \pm b$.

For the wall, $y = +b$, solutions of (2.1) generated in the interior which strike this wall are superpositions of special plane waves of the form (in these Fourier modes we specialize to $\xi > 0$ for simplicity),

$$\hat{\varphi}_-(\omega_1, \xi) = e^{i(\beta_- y + \omega_1 x + \xi t)}, \qquad \xi > 0, \tag{2.3}$$

where $\beta_\mp = \mp(2\omega_1\xi - K^*\omega_1)^{1/2} = \mp\xi(2n - K^*n^2)^{1/2}$ with $n = \omega_1/\xi$, $\hat{\varphi}_+$ is defined using β_+.

A boundary condition on the wall $y = b$ which annihilates the plane wave solution in (2.3) exactly for fixed (ω_1, ξ) is given by

$$\left(\frac{\partial}{\partial y} + i\xi(2n - K^*n^2)^{1/2}\right)\hat{\varphi}\,|_{y=b} = 0. \tag{2.4}$$

If we recall the correspondence (see [6, 7]) $i\xi = \partial/\partial t$, $i\omega_1 = \partial/\partial x$, valid under Fourier transformation, then (2.4) is the Fourier transform of the *theoretical perfectly radiating* boundary condition for the equation in (2.1) and the boundary, $y = b$. As it stands, this boundary condition is not practical because it is nonlocal simultaneously and time.

Next, we discuss approximating the boundary condition defined in (2.4) by local boundary conditions in a fashion dictated by the special wave propagation properties of (2.1). In particular, it follows from the remarks in (2.2) and Fig. 2 that effective radiating boundary condition in the "glancing regime,"

$$0 \approx \frac{\omega_1}{\xi} = n \ll 1 \tag{2.5}$$

are essential. Since we need to approximate $(2n - K^*n^2)^{1/2}$ near $n = 0$, the expansion methods used in [6, 7], do not apply directly. In the subsonic case, $(2n - K^*n^2)^{1/2}$

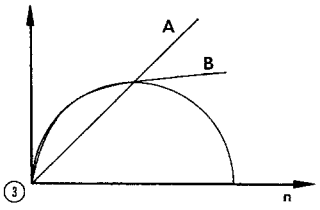

FIG. 3. Graph of $(2n - K^*n^2)^{1/2}$ and the approximations. A. (2.8). B. (2.9) for $K^* = 1$.

has the graph displayed in Fig. 3. The first approximate radiation boundary conditions which we use are based on the linear approximation

$$(2n - K^*n^2)^{1/2} \approx rn. \tag{2.6}$$

1st radiating boundary condition.

$$\varphi_y + r\varphi_x|_{y=b} = 0, \qquad r \geqslant 0. \tag{2.7}$$

The requirement, $r \geqslant 0$, is imposed by the stability analysis in Section 1. In the subsonic case, one effective strategy we have used to "tune" this radiating boundary condition is to choose r so that the corresponding straight line passes through the maximum value of $(2n - K^*n^2)^{1/2}$ resulting in

subsonic 1st radiating condition.

$$(\varphi_y + (K^*)^{1/2}\varphi_x)|_{y=b} = 0. \tag{2.8}$$

Higher order radiating boundary conditions can be developed by using better rational approximations to $(2n - K^*n^2)^{1/2}$ near $n = 0$ of the form,

$$(2n - K^*n^2)^{1/2} \approx \frac{r_1 n}{1 + r_2 n}.$$

The resulting general local second order radiating boundary conditions have the form,

2nd radiating boundary condition.

$$\varphi_{ty} + r_2\varphi_{xy} + r_1\varphi_{xt}|_{y=b} = 0. \tag{2.9}$$

Of course, strategies are needed to tune the radiating boundary conditions in (2.9) to reduce (unphysical) reflections and maintain stability. In the *subsonic* case, two simple strategies implemented in numerical experiments below are the following:

(1) Require $r_1 n/(1 + r_2 n)$ to interpolate $(2n - K^*n^2)^{1/2}$ through 0 and two other points, say $1/2K^*$, $1/K^*$; (2.10)

(2) Choose r_1, r_2 so that for a given n_0

$$\max_{0 \leqslant n \leqslant n_0} \left| (2n - K^* n^2)^{1/2} - \frac{r_1 n}{1 + r_2 n} \right|$$

is minimized.

An obvious appropriate scaling to use in any of the strategies in (2.10) is to guarantee that $r_1 = c_1 (K^*)^{1/2}$, $r_2 = c_2 (K^*)^{1/2}$, where c_1, c_2 are chosen by a fixed strategy independent of K^*.

We remark that in the supersonic case, $K^* < 0$, the graph of $(2n - K^* n^2)^{1/2}$ has a linear asymptote with slope $(-K^*)^{1/2}$ as $n \to \infty$. In this case, the above graph is well approximated by the straight line, $w = (-K^*)^{1/2} n$ so that the radiation boundary conditions,

supersonic 1st radiating condition

$$\varphi_y + (-K^*)^{1/2} \varphi_x |_{y=b} = 0 \tag{2.11}$$

are already quite efficient. We note that in the supersonic case, the above linearized approach does not take into account the fact that shock waves may form and strike $y = \pm b$ in the far field. However, the shock waves that occur within the validity of the transonic approximation in (0.1) are necessarily weak shocks and the argument of Hedstrom applies (see [8]).

Given a boundary condition, $\mathscr{B}(\varphi)|_{y=b} = 0$ for solutions φ of (2.1) and a plane wave $\hat{\varphi}_-$ of the form in (2.3) striking the wall $y = b$, the *reflection coefficient* is the number, $R(n)$, so that

$$\mathscr{B}(\hat{\varphi}_- + R(n)\, \hat{\varphi}_+)|_{y=b} = 0. \tag{2.12}$$

Obviously, the magnitude of the reflection coefficient, $|R(n)|$ is an analytic measure of the effectiveness of $\mathscr{B}$ as a radiating boundary condition (the smaller $|R(n)|$, the better the radiation boundary condition). For the boundary condition $\varphi|_{y=b} = 0$ used in [1, 5],

$$|R(n)| \equiv 1, \qquad 0 \leqslant n \leqslant \frac{2}{K^*},$$

so that this boundary condition *totally reflects* waves back into the interior with their magnitudes preserved. On the other hand, the most trivial subsonic 1st radiating boundary condition in (2.8) has

$$|R(n)| \equiv \left| \frac{-(2n - K^* n^2)^{1/2} + (K^*)^{1/2} n}{(2n - K^* n^2)^{1/2} + (K^*)^{1/2} n} \right|, \qquad 0 \leqslant n \leqslant \frac{2}{K^*}. \tag{2.13}$$

This number is substantially smaller than 1 for most $0 \leqslant n \leqslant 2/K^*$—by construction. $R(1/K^*) = 0$; $R(1/2K^*) = |(1 - 3^{1/2}/2)/(1 + 3^{1/2}/2)|$, etc. The higher order approx-

imations in (2.9) can be systematically tuned according to the strategies in (2.10) to substantially reduce $|R(n)|$ in (2.13) over the approximation defined in (2.8) in the subsonic case (see the numerical experiments in Section 4).

By symmetry, radiating boundary conditions on $y = -b$ (which are analogous to those in (2.7) and (2.9)) have the form,

$$\varphi_y - r_1 \varphi_x |_{y=-b} = 0, \qquad r_1 \geqslant 0,$$
$$\varphi_{yt} + r_2 \varphi_{yx} - r_1 \varphi_{xt} |_{y=-b} = 0.$$

The upstream boundary, $x = 0$

In the subsonic case, waves propagating from the interior and striking the boundary $x = 0$ are superpositions of the modes ($\xi > 0$ for simplicity)

$$\hat{\varphi}_+ = e^{i\lambda^+ x + i\xi t + i\omega_2 y}$$

and (2.14)

$$\hat{\varphi}_- = e^{i\lambda^- x + i\xi t + i\omega_2 y},$$

where

$$\lambda^+ = \frac{\xi + \xi(1 - K^*\beta^2)^{1/2}}{K^*}, \qquad \lambda^- = \frac{\xi - \xi(1 - K^*\beta^2)^{1/2}}{K^*}, \qquad \text{and} \qquad \beta = \frac{\omega_2}{\xi}.$$

The mode associated with $\hat{\varphi}_1$ carries information away from the computational region. The frequency dependent theoretical radiating boundary condition (with no reflections) is given by

$$\left(\frac{\partial}{\partial x} - i \frac{\xi + \xi(1 - K^*\beta^2)^{1/2}}{K^*} \right) \hat{\varphi} |_{x=0} = 0.$$

From Fig. 2, waves generated in the interior first strike $x = 0$ at normal incidence where $\beta = 0$. Thus, the standard Taylor expansion analysis used in [6, 7] applies directly since β near zero is important for the wall $x = 0$ yielding the following 1st and 2nd radiating conditions:

$$\varphi_t - \frac{K^*}{2} \varphi_x |_{x=0} = 0, \tag{2.15}$$

$$\varphi_{xt} - \frac{2}{K^*} \varphi_{tt} + \frac{1}{2} \varphi_{yy} |_{x=0} = 0. \tag{2.16}$$

The downstream boundary, $x = a$

In the subsonic case, the same two modes as in (2.14) influence wave propagation near this boundary; however, their roles are reversed. At $x = a$, the mode associated

with λ^+ transports unphysical reflections back into the region of calculation. On the other hand, waves reflect rapidly off the boundaries $y = \pm b$ near the downstream boundary $x = a$ (see Fig. 2) and effective radiating boundary conditions for the "glancing mode," λ^-, are important in order to avoid a large mass buildup. The theoretical radiating boundary condition for this mode is given by

$$\left(\frac{\partial}{\partial x} - i\frac{\xi - \xi(1 - K^*\beta^2)^{1/2}}{K^*}\right)\hat{\varphi}\,|_{x=a} = 0$$

From the Taylor expansion procedure in [6, 7] we formally arrive at the 1st and 2nd approximations,

$$\varphi_x\,|_{x=a} = 0, \tag{2.17}$$

$$\varphi_{xx}\,|_{x=a} = 0. \tag{2.18}$$

These conditions were introduced by Krupp and Cole in [5].

In the supersonic case, two boundary conditions ($\varphi = c_0, \varphi_2 = 0$) are needed upstream and no boundary conditions should be described downstream thus no analysis of radiating boundary conditions is necessary.

We conclude this section by remarking that the linearization of the equation in (0.1) about a solution, Φ, of (0.1) is given by

$$2\varphi_{xt} = (K - (\gamma + 1)\,\Phi_x)\,\varphi_{xx} + \varphi_{yy} - ((\gamma + 1)\,\Phi_{xx})\,\varphi_x,$$

i.e., the lower order term involving φ_x is also present. The theory developed in [6, 7] includes the design of radiating boundary conditions for equations with lower order terms. However, when 2nd variable coefficient radiating approximations are used, the practical reduction of error is modest for linear wave calculations (see [7]). For the nonlinear equation in (0.1), we expect most of this improvement to be lost anyway because of mild nonlinear effects in the far field. However, we expect a significant improvement in using the second approximations in (2.9) instead of the first ones in (2.7) as the numerical evidence in [6, 7] indicates.

3. Discretization of Radiating Boundary Conditions

We introduce the grid $\{(x_j, y_k, t^n)\}$, $x_j = j\,\Delta x$, $y_k = k\,\Delta y$, $t^n = n\,\Delta t$; $j = 0, 1, \ldots, J$; $k = -K, \ldots, K$, $n = 0, 1, 2, \ldots$; $\Delta x = a/J$, $\Delta y = b/K$. The solution $\varphi(x_j, y_k, t^n)$ at a grid point is approximated by the grid function $\varphi^n_{j,k}$. We use standard notation for the divided differences, D^x_+, D^x_-, D^y_+, etc. (for example, $D^x_+ \varphi^n_{j,k} = (\varphi^n_{j+1,k} - \varphi^n_{j,k})/\Delta x$).

We concentrate here on appropriate discretization of the radiation boundary onditions at the side walls, $y = \pm b$. First, we give some simple compact formulae for the 1st and 2nd radiating boundary conditions,

$$\begin{aligned} &\text{(a)} && \varphi_y \pm r\varphi_x\,|_{y=\pm b} = 0, \qquad r \geqslant 0, \\ &\text{(b)} && \varphi_{ty} + r_2\varphi_{xy} \pm r_1\varphi_{xt}\,|_{y=\pm b} = 0, \end{aligned} \tag{3.1}$$

derived in (2.7) and (2.9) above. A simple compact formula for (3.1a) (at $y = b$) is given by

$$D_-^y(\varphi_{j,K}^{n+1} + \varphi_{j-1,K}^{n+1}) + rD_-^x(\varphi_{j,K}^{n+1} + \varphi_{j,K-1}^{n+1}) = 0. \tag{3.2}$$

We remark that when explicit interior schemes are used, no matrix inversions are required. A useful compact formula for the second radiation boundary condition in (3.1b) (for the $y = b$ case) is given by

$$D_-^y D_-^t(\varphi_{j,K}^{n+1} + \varphi_{j-1,K}^{n+1}) + r_2 D_-^y D_-^x(\varphi_{k,K}^{n} + \varphi_{j,K}^{n+1}) + r_1 D_-^x D_-^t(\varphi_{j,K}^{n+1} + \varphi_{j,K-1}^{n+1}) = 0. \tag{3.3}$$

Next, we discuss implementing the radiating boundary conditions in (3.1) in the difference schemes used by Krupp and Cole and Ballhaus and Goorjian in [1, 5]. These difference schemes are typical examples of the ones used for computations in transonic flow. The difference schemes used in [1, 5] for the unsteady small disturbance equation both have the following properties: (1) Each is an implicit scheme containing two time levels. (2) There is no linear stability constraint on Δt but in practice nonlinear instabilities can occur with large Δt. (3) These schemes are type sensitive— different approximations are used in the subsonic and supersonic cases. The methods differ in the following respect: In [1] an ADI-splitting is used so that only systems with narrow bandwidth need to be inverted, while in [5] a larger system of equations must be solved at each time step.

The discrete artificial boundary conditions used by these authors are simple discrete analogues of those described in (1.6), (1.7), above:

$$\begin{aligned} &\text{at } k = \pm K, && \varphi_{j,k}^n = 0 && \text{(side walls)}, \\ &\text{at } j = 0, && \varphi_{0,k}^n = 0 && \text{(upstream)}, \\ &\text{at } j = J, && D_-^x \varphi_{J,k}^n = 0 && \text{or } (D_-^x)^2 \varphi_{J,k}^n = 0 \\ & && && \text{(downstream)}. \end{aligned} \tag{3.4}$$

The first approximate radiating boundary condition can be discretized by using (3.2). The scheme in (3.2) is fully implicit and can be changed to the unitary scheme (still implicit) using $\varphi^{n+1/2} = 1/2(\varphi^n + \varphi^{n+1})$, the result is

$$D_-^y(\varphi_{j,K}^{n+1} + \varphi_{j-1,K}^{n+1} + \varphi_{j,K}^{n} + \varphi_{j-1,K}^{n}) + rD_-^x(\varphi_{j,K}^{n+1} + \varphi_{j,K-1}^{n+1} + \varphi_{j,K}^{n} + \varphi_{j,K-1}^{n}) = 0. \tag{3.5}$$

Both of the approximations in (3.2) and (3.5) are second order accurate and can be used directly with the schemes in [1, 5] without any modification. We remark that the reflected errors in using the first order approximation in (3.1a) are not particularly sensitive to small changes in K^* so that r can often be kept constant—of course, the value of r can be made a function of the x-difference in φ.

Convenient approximations of the second order radiating boundary conditions in (3.1b) which are designed for use with the schemes in [1, 5] are given by (3.3).

The discretization of the upstream radiating boundary conditions at $x = 0$ from (2.15), (2.16) is standard following the techniques in [6, 7] so we omit a detailed

description here. At downstream bundaries the implementation in the schemes developed in [1, 5] is straightforward.

Numerical Experiments

In the numerical experiments we used a modified version of the ADI scheme of Cole–Murman type from [2]. The nonlinear x-sweep was, however, treated in a fully explicit fashion (for convenience); the y-sweep was kept implicit.

At $y = \pm b$, we implemented the 1st and 2nd radiating boundary conditions from (2.7) and (2.9) with the discretization from (3.2) and (3.3), respectively. In the strategy in (2.10), (1) was used. Upstream, we implemented a straightforward discrete version of the first radiating boundary condition in (2.15) (see [6, 7]). For purposes of comparison we also implemented the discrete boundary conditions from [1, 5] described in (3.4).

Below, we report on the numerical values resulting from a typical numerical experiment involving discrete solutions of (0.1). In this experiment, we used a free stream value $K \equiv 0.9$, a computational grid with 2000 points, and a C.F.L. condition of 0.5. For initial values we used a pulse with compact support and continuous first derivatives centered in the middle of the computational grid (a piece of a radially symmetric sine curve). After a short time the main energy in the pulse spreads out in a parabolic wavefront (see Fig. 2) and reflections occur at the computational boundaries. We looked at the resulting discrete solution after 200 time steps. The quantity measured below is the *maximum value of the reflected error normalized* so that it is $\equiv 1$ for the standard reflecting boundary conditions,

$$\varphi|_{y=\pm b} = 0, \qquad \varphi|_{x=0} = 0, \qquad \varphi_x|_{x=a} = 0.$$

We computed the reflected errors in all cases by solving the initial value problem on a much larger region and subtracting the two solutions.

Side Boundary ($y = \pm\ b$)

(Normalized normalized reflected error)

Boundary condition	$0 \leqslant x \leqslant a$	$0 \leqslant x \leqslant \frac{3}{4}a$
$\varphi = 0$	1.00	1.00
1st radiating b.c.	0.37	0.09
2nd radiating b.c.	0.18	0.06

We remark that in this experiment and all other numerical tests which we have made, the error downstream near $x = a$ builds up immediately but propagates very slowly into the computational region; thus, the maximum of the reflected errors is reduced even further by the 1st and 2nd radiating boundary conditions on a smaller domain such as $0 \leqslant x \leqslant \frac{3}{4}a$. If the coefficients of r_1 and r_2 are tuned in a time-dependent fashion, the errors in the full domain can be reduced further.

At the upstream boundary, $x = 0$, there is a substantial reduction in the reflected errors for φ using only the 1st radiating boundary condition and some improvement in φ_x.

Upstream Boundary ($x = 0$)

(Normalized maximum reflected error)

Boundary condition	reflection in φ	reflection in φ_x
$\varphi = 0$	1.00	1.00
1st radiating b.c.	0.08	0.38

At the downstream boundary, $x = a$, we compared the choices $\varphi_x|_{x=a}$ and $\varphi_{xx}|_{x=a} = 0$. The improvement in φ is modest but the gain in φ_x in this case is more substantial.

Downstream Boundary ($x = a$)

(Normalized maximum reflected error)

Boundary condition	reflection in φ	reflection in φ_x
$\varphi_x|_{x=a} = 0$	1.00	1.00
$\varphi_{xx}|_{x=a} = 0$	0.81	0.29

For a more detailed description of the reflection from the side boundaries, see the graph in Fig. 4 where the amplitude of the reflection at a fixed mesh point in space is plotted as a function of time for the boundary conditions $\varphi|_{y=\pm b} = 0$ used in [1, 5] and the 2nd radiating boundary condition described above.

Several calculations with different parameters were performed. The experiment described above is typical but the actual numbers may vary between different problems.

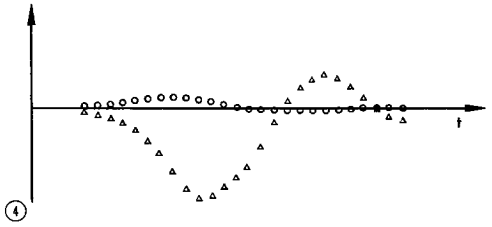

FIG. 4. The amplitude of the reflections from the side boundaries at a fixed mesh point in space is plotted as a function of time. The mesh point is located at the distance Δy from the side boundary. The boundary condition $\varphi|_{y=b} = 0$ (triangle) and the 2nd radiating boundary condition (2.9) (circle).

CONCLUSIONS

Using systematic principles, a family of far-field radiating boundary conditions for the small disturbance equation of unsteady transonic flow was derived. These discrete far-field boundary conditions are easily implemented with a variety of popular difference schemes for transonic flow. Both the analytic and numerical comparisons indicate substantial improvements over other currently used methods for treating such far-field boundaries.

Note added in proof. Also see the calculations reported by Kwak [9] for further experiments with these methods.

REFERENCES

1. W. F. BALLHAUS AND P. M. GOORJAN, "Implicit Finite Difference Computations of Unsteady Transonic Flows about Airfoils Including the Treatment of Irregular Shock Wave Motions," A.I.A.A. paper 77–205, 1977.
2. W. F. BALLHAUS AND H. LOMAX, *in* "Proceedings, Fourth International Conference on Numerical Methods in Fluid Dynamics (R. D. Richtmyer, Ed.), Lecture Notes in Physics No. 35, pp. 57–63. Springer–Verlag, Berlin/New York, 1975.
3. J. D. COLE, *SIAM J. Appl. Math.* **29** (1975), 763–787.
4. C. GROSCH AND S. ORSZAG, *J. Comp. Phys.* **25** (1977), 273–296.
5. J. A. KRUPP AND J. D. COLE, "Studies in Transonic Flow IV, Unsteady Transonic Flow," U.C.L.A. Eng. Report 76104, 1976.
6. B. ENGQUIST AND A. MAJDA, *Math. Comp.* **31** (1977), 629–651.
7. B. ENGQUIST AND A. MAJDA, *Comm. Pure Appl. Math.* **32** (1979), 313–357.
8. G. W. HEDSTROM, *J. Comp. Phys.* **30** (1979), 222–237.
9. D. KWAK, "Nonreflecting Far-Field Boundary Conditions for Unsteady Transonic Flow," A.I.A.A. paper 80-1393, 1980.